Comparison of Vibration-Dissociation Coupling and Radiative Transfer Models for AOTV/AFE Flowfields

Leland A. Carlson,* Glenn J. Bobskill,† and Robert B. Greendyke†
Texas A&M University, College Station, Texas

A series of detailed studies comparing various vibration-dissociation coupling models, reaction systems and rates, and radiative heating models has been conducted for the nonequilibrium stagnation region of an Aeroassisted Flight Experiment/aeroassisted orbital transfer vehicle. Atomic and molecular nonequilibrium radiation correction factors have been developed and applied to various absorption coefficient step models, and a modified vibration-dissociation coupling model has been shown to yield good vibration/electronic temperature and concentration profiles. Although the results indicate sensitivity to the choice of vibration-dissociation coupling model and to the nitrogen electron-impact ionization rate, accurate flowfield and radiative heating results can be obtained by careful modeling. The results indicate that nonequilibrium effects significantly affect the flowfield and the radiative heat transfer, and that additional work is needed in ionization chemistry and absorption coefficient modeling.

Nomenclature

A	= vibrational diffusive coefficient, Eq. (4)
A, B, E	= reaction rate coefficients, Eq. (1)
B_{pq}	= probability for a transition from state p to state q
B_ν	= black-body function
E_2	= exponential integral of type 2
g_p	= degeneracy for state p
h	= Planck's constant
I	= intensity [Eq. (8)] or ionization energy [Eq. (11)]
IR	= infrared region
k	= Boltzmann constant
$k_{f,b}$	= forward or backward reaction rate
K_i, K_ν	= absorption coefficient for band i or frequency ν
N	= number density
$N(p)$	= number of atoms in state p
q_r, QR	= radiative transfer to the wall, W/cm^2
RR1, RR2, RR3	= reaction chemistry sets, see Table 1
s	= superscript in Eq. (4), also distance coordinate in Eq. (8)
S_i, S_ν	= radiation source function for band i or frequency ν
T, TH	= heavy particle or translational temperature
T_e, TE	= electron temperature
T_{vN2}, TVN2	= N_2 vibrational temperature
x, y	= coordinates parallel and perpendicular to shock front
α	= degree of ionization, $N_I/(N_I + N_A)$
β	= degree of dissociation, $(N_A + N_I)/(N_A + N_I + 2N_M)$
$\beta_{pq}(\nu)$	= line shape function
ϵ	= vibrational energy
ϵ_p	= energy of state p
ν	= frequency
σ	= radiative cross sections
τ	= vibrational relaxation time [Eq. (3)] or optical thickness [Eq. (7)]

Subscripts

A	= atoms
e	= electron
eq	= equilibrium
E	= equilibrium conditions for local pressure and electron temperature
gc	= continuum to ground
i	= wavelength region i
I	= ion
j	= species j
j_∞	= species j at equilibrium conditions
M	= molecule
MW	= Millikan-White
pc	= continuum to state p
pq	= state q to state p
s	= conditions at shock front
ν	= frequency

Introduction

IN the future, aeroassisted orbital transfer vehicles (AOTV's) will be used to return from geosynchronous orbit, lunar, and Mars missions. Vehicles descending from geosynchronous to high or low Earth orbit will operate in the aerocapture mode at velocities of 7–11 km/s at altitudes of 70–100 km, with a nominal entry velocity of 10 km/s. To efficiently design such vehicles, the important factors affecting the vehicle flowfields must be understood and methods for rapidly predicting them must be available. For many designs, the forebody flow will be dominated by nonequilibrium chemistry and radiation, and these phenomena will greatly affect the heat transfer and perhaps the aerodynamics of the vehicle.

Detailed three-dimensional nonequilibrium viscous computations of AOTV flowfields will be required to obtain a complete understanding of the various phenomena. These computations, typically using the Navier-Stokes equations,[1] are extremely difficult and computationally intensive, and only a few[2] have included the effects of such nonequilibrium phenomena as vibration-dissociation coupling, electron thermal nonequilibrium, and radiative heat transfer. Because of their

Presented as Paper 88-2673 at the AIAA Thermodynamics, Plasmadynamics, and Lasers Conference, San Antonio, TX, June 27-29, 1988; received July 18, 1988; revision received Dec. 22, 1988.

*Professor of Aerospace Engineering. Associate Fellow AIAA.
†Graduate Research Assistant.

computational intensity, these detailed methods are often unsuitable for evaluating or developing models and approximations representing these nonequilibrium phenomena.

This paper discusses one portion of an effort to evaluate and develop models and approximations for nonequilibrium reacting and radiating flows associated with AOTV's and is applicable to entry velocities ranging from 7 to 10 km/s. The objectives of this effort have been to investigate and compare various vibration-dissociation chemistry coupling models and radiative heat-transfer approximations and to determine the similarities, differences, and consequences of using these models in the AOTV flight regime.

Flow Property Models

Flowfield Solution Method

In order to investigate various vibration-dissociation coupling and radiative heat-transfer models efficiently, the use of a rapid flowfield solver is essential. After considering various possibilities, it was decided to use an inviscid nonequilibrium chemistry axisymmetric inverse method[3] as the basic Euler equation flow solver. As part of the present study, this method has been modified and extended to include as options various vibration-dissociation coupling, shock jump, radiative heat transfer, and electron temperature models. This method is computationally efficient, permits the study of user-selected streamlines when the entire flowfield is not needed, and has been used in the present study to model the forward face of the Aeroassisted Flight Experiment (AFE) vehicle as a 60-deg axisymmetric blunt cone having a nose radius of 230 cm.[4]

Reaction Systems and Rates

In this investigation, two different chemical reaction systems have been considered. The first uses 7 species and 6 reactions, and the second is composed of 10 species and 11 reactions. Since computational effort is directly related to the number of species and reactions, it was hoped that by comparing results obtained with these two schemes that flight regimes where simple schemes would be adequate could be determined. For the second system, the effects of three different electron-impact nitrogen-ionization rates have also been investigated since previous studies[5,6] have indicated that this reaction dominates air ionization. These four reaction schemes are based on experimental and analytical data from Refs. 5-10, and their reactions and rates are listed in Table 1. In all cases, the rate constants are of the form

$$k_{f,b} = AT^B e^{-E/T} \tag{1}$$

The value of E in reactions (9-11) in set RR2 is based on the assumption that nitrogen ionization is limited by initial excitation to the $3s^4P$ state.[5] It should be noted that, for sets RR2A, RR2, and RR3, the predicted rates for reaction (11) for a given temperature each differ by an order of magnitude, with that for RR3 being the fastest.

Vibration-Dissociation Coupling Models

For vibration-dissociation coupling, it has been assumed that the vibrational energy of the jth diatomic species, ϵ_j, can be described schematically by

$$\frac{d\epsilon_j}{dt} = \frac{\epsilon_{j\infty} - \epsilon_j}{\tau_j} A - \text{term 2} + \text{term 3} \tag{2}$$

where the first term describes the rate of change of vibrational energy due to collisions, the second term represents the average energy lost from vibration due to a single dissociation, and the third term accounts for the average energy gained by vibration in a single recombination. In addition, the effect of vibration on dissociation is accounted for via a vibrational coupling factor, $V = k_{f\,\text{actual}}/k_{f\,\text{eq}}$, which relates the actual forward dissociation rate to that which would occur if the flow were in vibrational equilibrium. Complete details concerning the actual forms of the terms in Eq. (2) and of the vibrational coupling factor are given in Refs. 7 and 11.

In the present study, five vibration-dissociation coupling models have been used. The first four are listed next.

1) Vibrational Equilibrium (VEQ) Model—In this case, complete vibrational equilibrium is assumed, all vibrational temperatures are equal to the translational temperature, Eq. (2) is not used, and the coupling factor is 1.

2) Coupled Vibration-Dissociation (CVD) Model[12]—Here all diatomic species are permitted to be in vibrational nonequilibrium; but only the first term of Eq. (2) with $A = 1$ and the vibrational coupling factor are used, and an equal probability of dissociation from each vibrational level in a sufficiently energetic collision is assumed. Thus, this model includes only the effects of vibration on dissociation.

3) Coupled Vibration-Dissociation-Vibration (CVDV) Model[7,11]—In this model, all of the terms in Eq. (2) are in-

Table 1 Reaction system models

Reaction	A	B	E	Ref. No.	Effective temperature
	Reaction rate set 1 (RR1)				
1. $2N+M \rightarrow N_2+M$	5.00E19	−1.5	0	7	T
2. $O_2+M \rightarrow 2O+M$	1.19E21	−1.5	59,380	7	T
3. $NO+M \rightarrow N+O+M$	5.18E21	−1.5	75,490	7	T
4. $N+O_2 \rightarrow NO+O$	1.00E12	0.5	3,120	7	T
5. $O+N_2 \rightarrow NO+N$	5.00E13	0.0	38,016	7	T
6. $NO^+ + e \rightarrow N+O$	1.80E21	−1.5	0	7	T
	Reaction rate set 2 (RR2)				
All of RR1 plus					
7. $N+N \rightarrow N_2^+ + e$	1.40E13	0	67,800	9	T
8. $O+M \rightarrow O^+ + e + M$	2.77E12	0.5	157,500	10	T
9. $N+N^+ \rightarrow 2N^+ + e$	2.34E11	0.5	120,000	6	T
10. $N+N \rightarrow N^+ + e + N$	2.34E11	0.5	120,000	6	T
11. $N+e \rightarrow N^+ + 2e$	4.16E13	0.5	120,000	5,6	T_e
	Reaction rate set 2A (RR2A)				
All of RR2 except last reaction replaced by					
11. $N+e \rightarrow N^+ + 2e$	2.70E13	0.5	168,800	10	T_e
	Reaction rate set 3 (RR3)				
All of RR2 except last reaction replaced by					
11. $N+e \rightarrow N^+ + 2e$	1.10E32	−3.14	169,000	9	T_e

cluded along with the vibrational coupling factor, and $A = 1$. However, the assumption of equal probability of dissociation from each vibrational level is retained. Since this model includes the physically important effects of dissociation on vibration as well as the reverse, it should be significantly better than CVD.

4) Preferential (CVDV-P) Model[7]—In this case, dissociation is assumed to occur with a greater probability or, preferentially, from the higher vibrational levels; the terms in Eq. (2) and the vibrational coupling factor are appropriately reformulated using partition functions and an anharmonic oscillator energy representation. Since this model delays dissociation until the upper molecular vibrational levels are populated, its use should yield more extensive nonequilibrium than the previous models. Again, $A = 1$.

Recently, Park[2,13] developed a new vibrational coupling model involving a combination of the electron, electronic, and vibrational energy equations assuming that the temperatures characteristic of all three energy modes are equivalent. This latter assumption is based on the existence of strong coupling between vibration and electrons[14] and has been observed experimentally.[8] In addition, Park modified the first term of Eq. (2) to account for two important effects. First, since the vibrational relaxation time correlations typically used[15] do not follow the Landau-Teller form, at high temperatures they predict unrealistically short relaxation times and imply unreasonably large cross sections. Consequently, Park modified the relaxation time to be the sum of two terms; the first is the usual form,[15] and the second is a limiting value based on a limiting cross section. The second Park modification accounts for the diffusive nature of vibrational relaxation at high temperatures and is incorporated via a coefficient on the collisional term in Eq. (2). This coefficient causes the vibration relaxation rate to vary nonlinearly with the difference in vibrational energies.[2,13,14] Finally, instead of using a vibrational coupling coefficient to reduce the forward dissociation rates, Park used an "average" temperature $\sqrt{T T_v}$ in the forward rate equations.

In the present study, a modified form of the CVDV coupling model, which includes the Park modifications for relaxation time cutoff and the effective diffusive coefficient, has been developed. However, this model uses only the vibrational energy equation, Eq. (2); and instead of the "average" temperature developed by Park, the model retains the use of the equivalent CVDV vibrational coupling factor to couple dissociation to vibration and to reduce the forward dissociation rates. In addition, the modifications are applied only to nitrogen vibrational relaxation. Thus, the fifth vibration-dissociation coupling model is listed next.

5) Modifed Coupled Vibration-Dissociation-Vibration (MCVDV) Model—In this pseudo-Park model, the nitrogen vibrational relaxation time in Eq. (2) is

$$\tau = \tau_{MW} + \frac{1}{NC\sigma_v} \tag{3}$$

where $C = \sqrt{8kT/\pi m}$ and $\sigma_v = (1.E-17)(50{,}000/T)^2$, and the coefficient A for nitrogen relaxation is

$$A = \left|\frac{T - T_v}{T_s - T_{vs}}\right|^{s-1} \tag{4}$$

where the exponent is[2,13]

$$s = 3.5 \exp(-5000/T_s) \tag{5}$$

For O_2, the usual CVDV equation is utilized since oxygen dissociation will occur extremely rapidly at the present conditions of interest. Also, the standard CVDV vibrational coupling factor is used to reduce the forward dissociation rates.

Radiative Heat-Transfer Models

For the 7–10-km/s AOTV/AFE flight regime, radiative heat transfer and self-absorption effects should be important, but the total radiative losses from the flowfield should be too small to induce any significant gasdynamic coupling. Thus, once a flowfield solution has been obtained for a given reaction rate system and vibration-dissociation coupling model, the flowfield solution can be used to compute the body radiative heat transfer for several radiative heat-transfer models. In the present study, the tangent slab approximation has been used for all of the radiative heat-transfer calculations. According to this approximation, the radiative flux to the surface is determined by the flow properties along a line perpendicular to the surface of the vehicle and, assuming that the surface is nonemitting and that no precursor effects are present, is given by

$$q_r(0) = 2\pi \sum_i \int_0^{\text{shock}} S_i(y) E_2\left[\tau_i(y)\right] K_i(y)\, dy \tag{6}$$

where the integration over the nongray spectrum has been approximated by a summation over a series of gray gas steps. Also, the optical thickness in terms of the absorption coefficient is

$$\tau_i(y) = \int_0^y K_i(y)\, dy \tag{7}$$

Since the present solution method is inviscid, all of the radiative heat-transfer results obtained in this study should be viewed as the radiative flux to the body boundary layer.

In evaluating Eq. (6), it would be convenient to determine the radiative cross sections and the absorption coefficients using previously determined gray gas step models.[16–18] However, these models were developed assuming chemical and thermal equilibrium, and must be modified or corrected before they can be applied to nonequilibrium flows. If excited electronic states were populated according to a Boltzmann distribution at the local electron temperature, i.e., local thermodynamic equilibrium (LTE), such models could be corrected by simply using the local electron temperature and nonequilibrium species concentrations to evaluate the cross sections and absorption coefficients. However, nitrogen and oxygen ionization is a two-step process involving excitation to an excited state followed by rapid ionization,[5] in which it can be assumed that the excited states are in local equilibrium with the electrons and ions. Consequently, in the nonequilibrium portions of the flow, the populations of the electronic states will not be those predicted by an LTE assumption, and additional corrections are needed. Park[2,13,19] has developed detailed models to predict these populations, and his results indicate that nonequilibrium effects are important for both atoms and molecules.

Now, in general, the equation of radiative transfer is

$$\frac{dI_\nu}{ds} = K_\nu(S_\nu - I_\nu) \tag{8}$$

where, for atomic continuum processes,[20,21]

$$K_\nu(p) = N(p) h\nu B_{pc}\left[1 - \left(N(p)_E/N(p)\right) e^{-h\nu/kT}\right] \tag{9}$$

$$S_\nu = \left(N(p)_E/N(p)\right)\left(2h\nu^3/c^2\left(e^{h\nu/kT} - N(p)_E/N(p)\right)\right)^{-1} \tag{10}$$

where subscript E indicates that state p is in equilibrium with the ions and electrons at the local pressure and electron temperature, i.e.,

$$N(p)_E = \frac{N_e N_I g_p h^3 e^{(I-\epsilon_p)/kT_e}}{2(2\pi m_e kT_e)^{3/2} Q_{eI}} \tag{11}$$

In an equilibrium step model, the atomic absorption coefficient and cross sections are normally expressed as

$$K_\nu = N_A \sigma_{\nu_{pc\,eq}} \tag{12}$$

and at equilibrium

$$N(p) = N(p)_E = N_A(g_p/Q_A)e^{-\epsilon_p/kT_e}$$

$$N(1) \cong N_A \qquad (\text{if } \epsilon_2/k \gg T_e) \tag{13}$$

So for p an excited state in equilibrium

$$\sigma_{\nu_{pc\,eq}} = \frac{h\nu B_{pc}(1-e^{-h\nu/kT_e})}{(Q_A/g_p)e^{\epsilon_p/kT_e}} \tag{14}$$

and p a ground state in equilibrium

$$\sigma_{\nu_{gc\,eq}} = h\nu B_{pc}\left[1-e^{-h\nu/kT_e}\right] \tag{15}$$

For atomic continuum processes involving the ground state, $N(p)=N(1)\cong N_A$, and the correction depends on the ratio of $N(1)_E/N(1)$. By using Eq. (11) with $p=1$, expressing the number densities in terms of the degrees of dissociation and ionization, and using the law of mass action to introduce α_{eq} and β_{eq}, the ratio becomes

$$\frac{N(1)_E}{N(1)} = \frac{(\beta\alpha^2)(1-\alpha_{eq})}{(1-\alpha)(\beta_{eq}\alpha_{eq}^2)} \tag{16}$$

Thus, for atomic continuum processes involving the ground state

$$K_\nu(1) \cong N_A\sigma_{\nu_{gc\,eq}} \tag{17}$$

assuming $\exp(-h\nu/kT)$ small in Eqs. (9) and (15); i.e., for such processes, equilibrium cross sections need not be modified.

However, the source function [Eq. (10)] becomes approximately

$$S_{\nu_{gc}} = \frac{\beta\alpha^2}{1-\alpha}\frac{1-\alpha_{eq}}{\beta_{eq}\alpha_{eq}^2}B_\nu \tag{18}$$

if $\exp(h\nu/kT) \gg N(p)_E/N(p)$.

Since it is assumed that excited states are in local equilibrium with ions and electrons, then for atomic continuum processes involving an excited state p, $N(p)=N(p)_E$ and

$$S_{\nu_{pc}} = B_\nu \tag{19}$$

Furthermore, by introducing Eq. (11) into Eq. (9), expressing N in terms of α and β, multiplying and dividing by N_A, and using the law of mass action to introduce α_{eq} and β_{eq}, the absorption coefficient becomes

$$K_\nu(p) = \frac{\beta\alpha^2}{1-\alpha}\frac{1-\alpha_{eq}}{\beta_{eq}\alpha_{eq}^2}\frac{N_A h\nu B_{pc}(1-e^{-h\nu/kT_e})}{(Q_A/g_p)e^{\epsilon_p/kT_e}}$$

$$= \frac{\beta\alpha^2}{1-\alpha}\frac{1-\alpha_{eq}}{\beta_{eq}\alpha_{eq}^2}N_A\sigma_{eqpc} \tag{20}$$

Thus, for atomic continuum processes involving excited states, the source function is the black-body function and the equilibrium absorption cross sections can be corrected for nonequilibrium effects.

For atomic line radiation, it was shown in Ref. 20, where p is the lower state, that

$$K_{\nu_{pq}} = N(p)B_{pq}\beta_{pq}(\nu)h\nu\left[1-\frac{N(q)}{N(p)}\frac{g_p}{g_q}\right] \tag{21}$$

$$S_{pq} = \frac{N(q)}{N(p)}\frac{g_p}{g_p}\frac{2h\nu^3}{c^2}\left[1-\frac{N(q)}{N(p)}\frac{g_p}{g_q}\right]^{-1} \tag{22}$$

If the process does not involve the ground state, and since excited states are assumed in equilibrium at the local electron temperature,

$$\frac{N(q)}{N(p)}\frac{g_p}{g_q} = e^{-h\nu/kT_e} \tag{23}$$

and

$$S_{\nu_{pq}} = B_{\nu_{pq}} \tag{24}$$

Since for this case $N(p)=N(p)_E$—following the same procedure as before—Eq. (11) can be used in Eq. (21) to yield

$$K_{\nu_{pq}} = \frac{\beta\alpha^2}{1-\alpha}\frac{1-\alpha_{eq}}{\beta_{eq}\alpha_{eq}^2}N_A\sigma_{pqeq} \tag{25}$$

where

$$\sigma_{pqeq} = \left[g_pB_{pq}\beta_p(\nu)h\nu(1-e^{-h\nu/kT_e})e^{-\epsilon_k/kT_e}\right]/Q_A$$

Likewise, if the lower state is a ground state and the upper state is an excited state, $N(p)=N(1)\cong N_A$, and if $\exp(-h\nu/kT_e)$ is small, then the cross section is uncorrected and

$$K_{\nu_{pq}} = N_A\sigma_{pqeq} \tag{26}$$

However, $N(q)$ will be in equilibrium with the ions and electrons. Again, using Eq. (11), introducing α and β, and removing terms via the law of mass action, Eq. (22) becomes

$$S_{\nu_{pq}} = \frac{\beta\alpha^2}{1-\alpha}\frac{1-\alpha_{eq}}{\beta_{eq}\alpha_{eq}^2}\frac{2h\nu^3}{c^2}\left[e^{h\nu/kT_e}-\frac{\beta\alpha^2}{1-\alpha}\frac{1-\alpha_{eq}}{\beta_{eq}\alpha_{eq}^2}\right]^{-1} \tag{27}$$

which can be approximated as

$$S_{\nu_{pq}} = \frac{\beta\alpha^2}{1-\alpha}\frac{1-\alpha_{eq}}{\beta_{eq}\alpha_{eq}^2}B_\nu \tag{28}$$

For molecules, a simlar local thermodynamic nonequilibrium condition will exist if it is assumed that the electronically excited molecules are in equilibrium with their atom counterparts at the local pressure and temperature. The latter essentially assumes that dissociation is dominated by collisional phenomena. Then, following a procedure similar to that for atomic lines, correction factors for molecular bands can be obtained. As for atomic lines, the source function is simply the black-body function, and the absorption coefficient becomes

$$k_{mol} = \frac{\beta^2(1-\alpha)^2}{1-\beta}\frac{1-\beta_{eq}}{\beta_{eq}^2(1-\alpha_{eq})^2}N_{mol}\sigma_{mol,eq} \tag{29}$$

It should be noted that Park[22] used a similar approach for molecular radiation called a "Z-distribution," which did not yield good spectral agreement with experimental data. However, his later detailed results[19] showed that during chemical nonequilibrium the excited states of N_2 are not in local thermodynamic equilibrium. In addition, the Fire2 data,[23] while detecting nonequilibrium molecular radiation, measured intensities much lower than expected. These facts, combined with the results to be discussed, indicate that Eq. (29), although approximate, is better than no correction at all.

Since cross sections and source functions for gray gas models are obtained by integrating over wavelength regions, and because these correction factors are wavelength independent, they can be applied directly to the individual steps of such models as long as the processes represented by a given step are of the same type (i.e., continuum involving excited states, lines, etc.). In addition, although the preceding corrections apply strictly to a single type of gas (i.e., nitrogen or oxygen), they can be applied approximately to air by defining separate degrees of dissociation and ionization for nitrogen and oxygen and by computing separate correction factors for the nitrogen and oxygen.

As indicated earlier, several different models have been incorporated into the present flowfield solution method to compute the radiative heat transfer to the vehicle. The simplest of these is an optically thin radiance model[24] that accounts for 13 different phenomena, including molecular bands, nitrogen and oxygen free-bound and bound-bound processes, and various free-free phenomena. In addition, three different nongray gas step models, which account for the effects of self-absorption in the computation of the heat transfer, have been included. Two of these models, a two-step[25] and a five-step[16] model, are based on high-temperature atomic nitrogen and should be representative of high-temperature air at temperatures above 8000–10,000 K. The third model, however, uses eight steps,[17] was developed for high-temperature air, and includes both atomic and molecular emission-absorption. The wavelength regions for these models are shown in Table 2. In all cases, the nonequilibrium correction factors discussed earlier have been included as appropriate. In addition, based on simplicity and experimental and analytical results,[2,8,14] the electron temperature has been assumed equal to the N_2 vibrational temperature. Since Eq. (2) includes only vibrational energy, this approach assumes that vibrational processes strongly influence the electron temperature but that the electrons have only a small influence on the vibrational energy.

Cases Considered

In the present study, results have been obtained for the 230-cm nose radius, 60-deg sphere cone at the three trajectory points listed in Table 3 for various combinations of reaction chemistry systems and vibration-dissociation coupling models. For the vibrational studies, 45 flowfield solutions, each involving 23 streamlines, were obtained; for the radiation comparisons, more than 20 cases, each using 43 streamlines, were computed. In the latter, the finer grid was required in order to resolve adequately the flowfield between the shock and the body. In all, over 30 charts were created; obviously, not all of these results can be discussed. Consequently, chemistry results will be presented only for the streamline (denoted as streamline 1.5) that crossed the shock front 1.5 cm above the axis, and radiation predictions will be shown for the body point 9 cm above the axis and discussed in terms of the flow between the shock and the body at that point. The trajectory for streamline 1.5, which typically contained 400–600 computational points for the length shown, is portrayed in Fig. 1 along with the shock and body locations. As can be seen, the present results are in the stagnation region of the vehicle.

Table 2 Radiation step models

Band	Wavelength A	Wavelength eV	Includes
		Eight-step model	
1	400–852	14.56–31.00	VUV continuum
2	852–911	13.62–14.56	VUV continuum
3	911–1020	12.16–13.62	VUV continuum
4	1020–1130	10.98–12.16	VUV continuum
5	1130–1801	6.89–10.98	Continuum + line wings
6	1130–1801	6.89–10.98	Line "centers"
7	1801–4000	3.10–6.89	"Visible"
8	4000–∞	0–3.10	Visible + infrared
		Five-step model	
1	620–1100	11.27–20	VUV continuum
2	1100–1300	9.54–11.27	VUV continuum
3	1300–1570	7.90–9.54	VUV lines
4	1570–7870	1.58–7.90	Visible
5	7870–9552	1.30–1.58	IR lines
		Two-step model	
1	0–1100	11.27–∞	VUV
2	1100–∞	0–11.27	Visible

Chemistry/Vibration Model Studies

7.71 km/s, 80 km

Typical results for streamline 1.5 for this trajectory point are shown in Fig. 2 for the MCVDV model and the RR3 reaction rate set. For a given vibration-dissociation coupling model, the T_{vN2} and nonionized species concentration profiles at this point are independent of which reaction rate chemistry set is used, and excellent results for these variables can be obtained with one-third the computational effort by using the 7-species, 6-reaction RR1 set. However, for ions and electrons, the simple RR1 set is inadequate, and the expanded systems, RR2 and RR3, are required. Interestingly, as portrayed in Fig. 3, the electron concentation predicted using the MCVDV model is relatively insensitive to the nitrogen-ionization electron-impact rate differences between RR2 and RR3, primarily due to the dependence of this rate on electron-vibrational temperature and the lower values predicted for them by the MCVDV model.

These temperatures are shown in Fig. 4, and the predicted T_{vN2} values are dependent on the vibration-dissociation coupling model used in the computations. Compared to the other models, the MCDVD model predicts a cooler T_{vN2} profile having a significantly lower peak value that occurs further downstream. In addition, comparison of concentration profiles reveals—at least for the RR2 set—that they are very similar for the MCVDV and CVDV-P models; this trend is displayed in Fig. 5 for N_2. Interestingly, experimental results[8,26] indicate that T_e only slightly overshoots its downstream value, that it peaks later than the T_{vN2} peak predicted using a CVDV-P model,[8] and that concentrations computed using CVDV-P predict intensity profiles in agreement with the measurements. Since MCVDV predicts a reasonable T_e profile via T_{vN2}, and concentrations very similar to those obtained using CVDV-P, it appears that the MCVDV model should be a good model for predicting electron temperatures and concentrations at this trajectory point.

10 km/s, 80 km

General results for streamline 1.5 for this case are shown in Fig. 6. These have been obtained using the MCVDV vibration-dissociation coupling model with the RR3 reaction set, and when compared to the 7.7-km/s results they indicate, as expected due to the higher freestream velocity, that this flow is approaching equilibrium faster than the previous one. Also,

Table 3 Trajectory points

Point	P_∞, dyne/cm^2	T_∞, K	U_∞, km/s	Approx. H, km
Entry	10.350	180.650	10.000	80
"Max-Q"	15.715	197.101	8.915	75
Exit	10.350	180.650	7.710	80

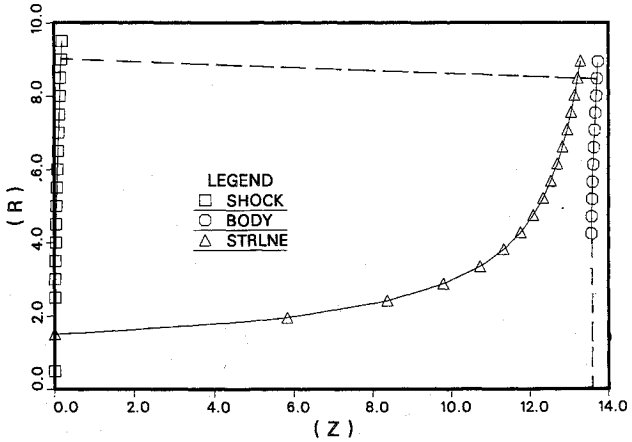

Fig. 1 Typical trajectory of streamline 1.5 at 10 km/s and 80 km.

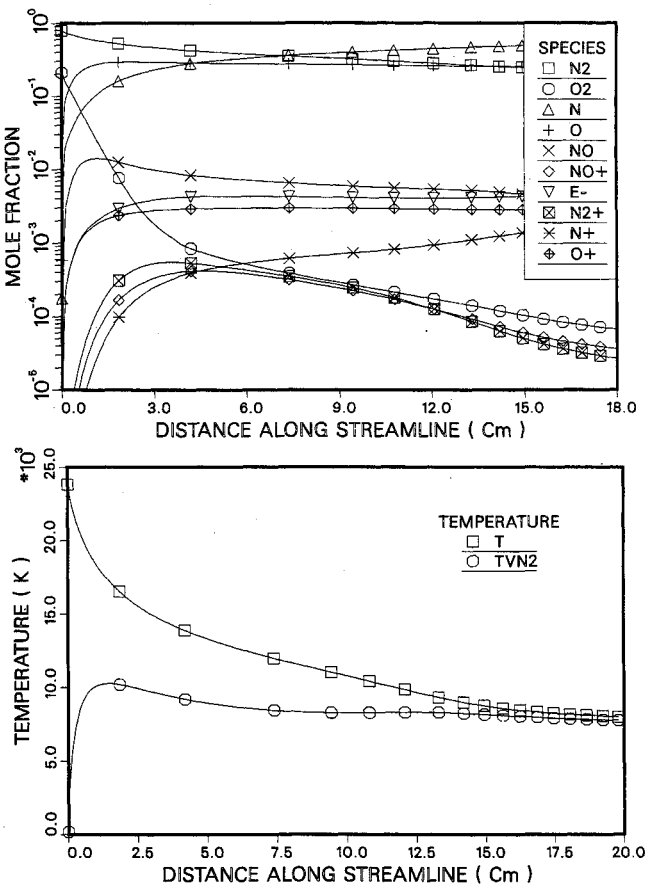

Fig. 2 Species and temperature profiles for MCVDV coupling and RR3 rates at 7.71 km/s.

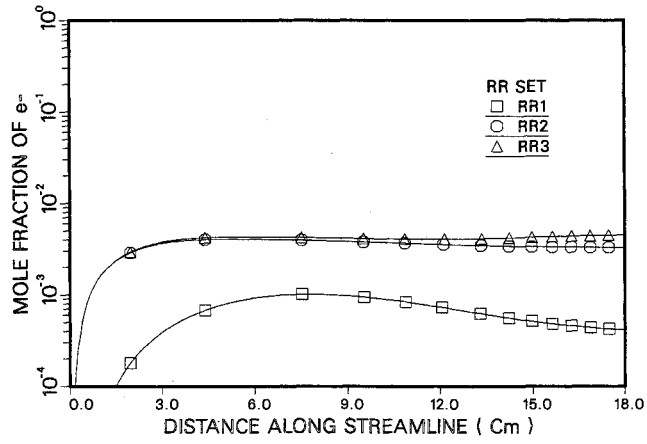

Fig. 3 Variation of electron concentration with reaction chemistry at 7.71 km/s using MCVDV coupling.

the species profiles show that the concentrations of nitrogen ions and electrons are significant; although not shown, comparison with the RR2 and RR3 results indicates that the simple RR1 system at this speed underestimates the electron concentrations by one or two orders of magnitude. Since the number of electrons and nitrogen ions strongly influences the number of atoms in excited states and, hence, the radiation, the expanded 10-species, 11-reaction chemistry system is needed at this trajectory point.

As shown in Fig. 7 for N_2, this case is similar to the previous one in that, for many of the species, the concentration profiles predicted by the CVDV-P and MCVDV models using the RR2 reaction rates are virtually identical. However, as portrayed in

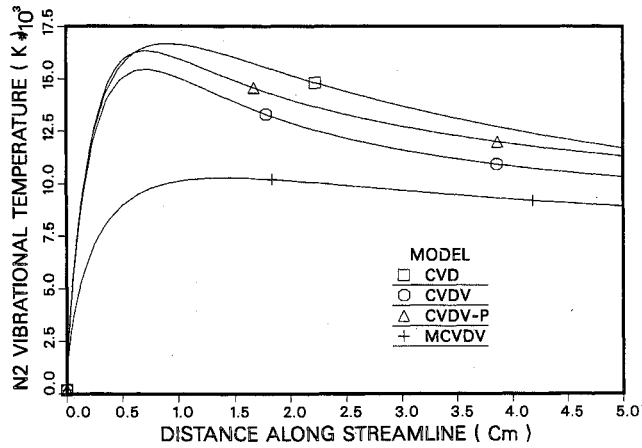

Fig. 4 Effect of vibrational model on T_{vN2} at 7.71 km/s using RR2 rates.

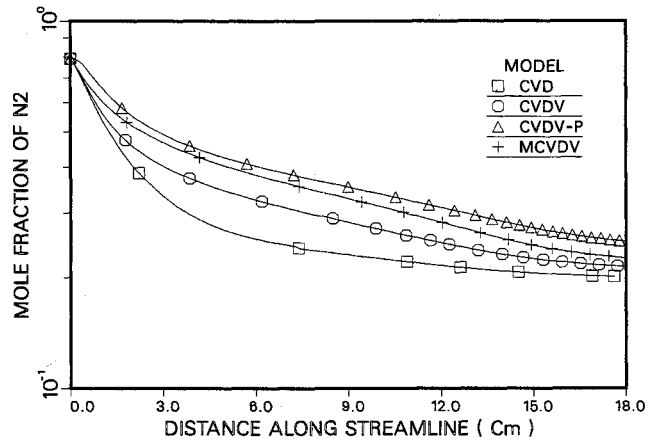

Fig. 5 Effect of vibrational model on N_2 concentration at 7.71 km/s using RR2 rates.

Fig. 8, although the T_{vN2} results for the CVDV-type models are similar, the profile from the MCVDV model is significantly cooler and, based on experiments at lower speeds and analyses at higher velocities,[6,8] perhaps a more realistic indicator of electron temperature. Of course, since nitrogen ionization is dominated by electron impact (reaction 11), which is controlled by T_e, these different electron temperature values significantly affect the N^+ concentrations. As depicted in Fig. 9 for RR2 rates, the N ion concentratons from MCVDV are less than one-half those predicted by CVDV and CVDV-P, although the electron concentrations for all three models are very similar.

In contrast to the RR2 results in Fig. 8, the T_{vN2} profiles predicted using the RR3 reaction rate set are, as shown in Fig. 10, similar along much of the streamline and independent of the vibration-dissociation coupling model. Only the CVD results—which actually overshoot the translational temperature and are probably physically incorrect—and the peak values are different. As mentioned previously, the peak value from MCVDV is probably more realistic if T_{vN2} is to be used for T_e.

Studies concerning the effects of reaction rates have been conducted for this condition and have concentrated on the effect of the nitrogen electron-impact ionization rate (RR2 vs RR3). Although not shown, comparison of the N^+ profiles shows significant differences between the RR2 and RR3 results, with the RR3 values being higher. Recall that the RR3 system is based on a one-step ionization process, whereas the RR2 set assumes a two-step sequence. Since the present solution scheme determines species production rates assuming that the reactions are single step, the RR3 rate set may be more compatible. Nevertheless, for the MCVDV model, Fig. 11

shows that T_{vN2} is relatively insensitive to the reaction rate scheme.

For the CVDV model, however, the high peak electron temperature shown in Fig. 10 leads to significant reaction rate sensitivity, as shown in Fig. 12 for the N atom concentration. In this case, as soon as a significant number of electrons are produced, the high electron-impact ionization rate in RR3 leads to electron avalanche and a rapid depletion in the N atom concentration, with the consequence that the predicted N concentration using RR3 is significantly lower than that predicted by the other rates throughout much of the flowfield. This sudden depletion in N also induces oscillations in the NO^+ and N_2^+ profiles when the CVDV model is used. It should be noted that such oscillations are not present in the MCVDV/RR3 results, probably because of the lower T_{vN2} values used for T_e in the electron-impact reaction.

Although firm conclusions may be presumptuous, it appears, based on results at this trajectory point, that the MCVDV model yields T_{vN2} profiles that can be realistically used for electron temperature. Also, the combination of MCVDV coupling and the RR3 reaction set yields reasonable concentration profile variations.

8.915 km/s, 75 km

Complete results for streamline 1.5 at this trajectory point are given in Fig. 13, and comparison with the 7.7-km/s results indicates that the chemical relaxation distance for this case is shorter, as would be expected considering the increase in both freestream pressure and velocity. On the other hand, comparison with the 10-km/s data in Fig. 6 shows that although the flow at 8.915 km/s is slightly cooler, the extent of nonequilibrium is about the same due to the competing effects of decreasing velocity and increasing ambient pressure. In addition, it can be seen in Fig. 13 that this case has extensive ionization, and the extended reaction chemistry sets involving 10 species and 11 reactions are needed to obtain accurate nonequilibrium chemistry and radiation results.

Like the entry point, the results at the max-Q point are sensitive to the reaction sets and the electron-impact ionization rates. For the CVDV model, the species profiles for N_2, N, O_2, NO, and O obtained using the RR3 values are significantly different from those obtained using RR1 and RR2, which are practically identical. On the other hand, the profiles for the same species predicted by the MCVDV model are insensitive and the same for RR1, RR2, and RR3. The charged species

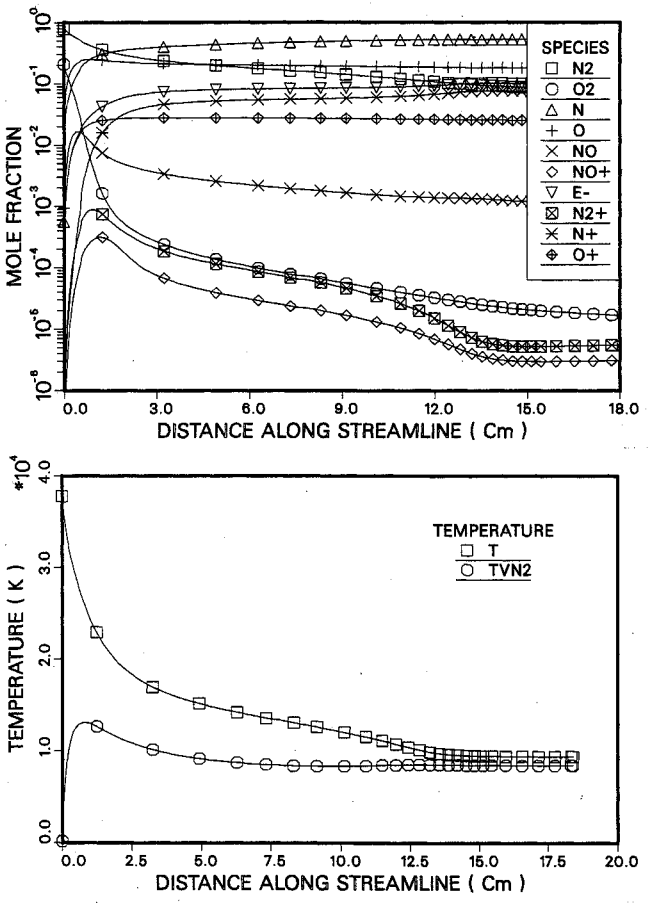

Fig. 6 Species and temperature profiles for MCVDV coupling and RR3 rates at 10 km/s.

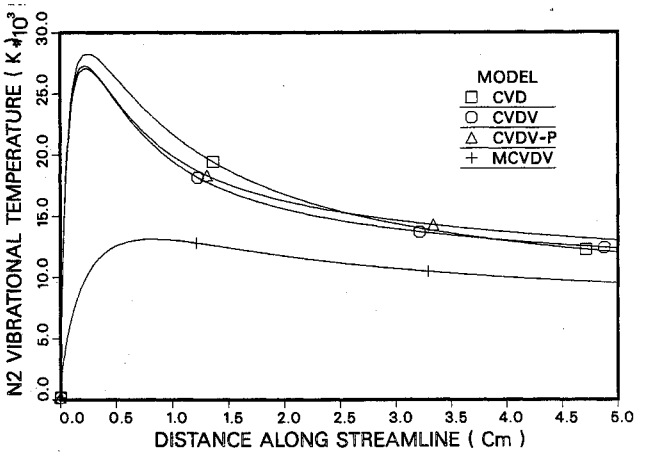

Fig. 8 Effect of vibrational model on T_{vN2} at 10 km/s using RR2 rates.

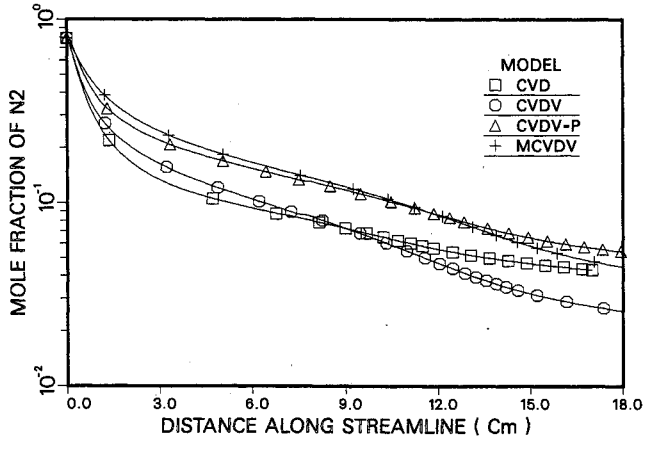

Fig. 7 Effect of vibrational model on N_2 concentration at 10 km/s using RR2 rates.

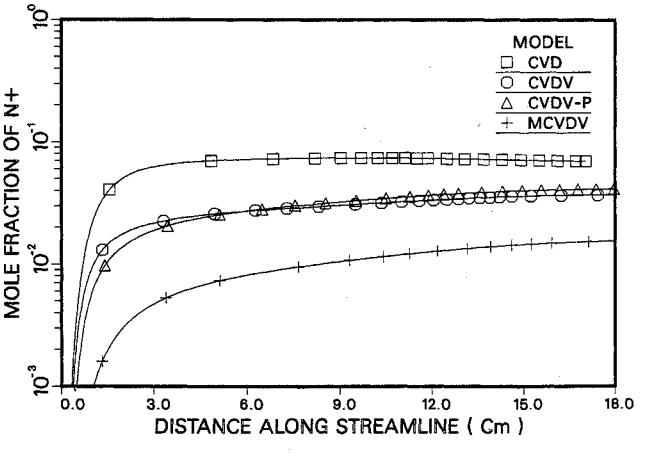

Fig. 9 Effect of vibrational model on N^+ concentration at 10 km/s using RR2 rates.

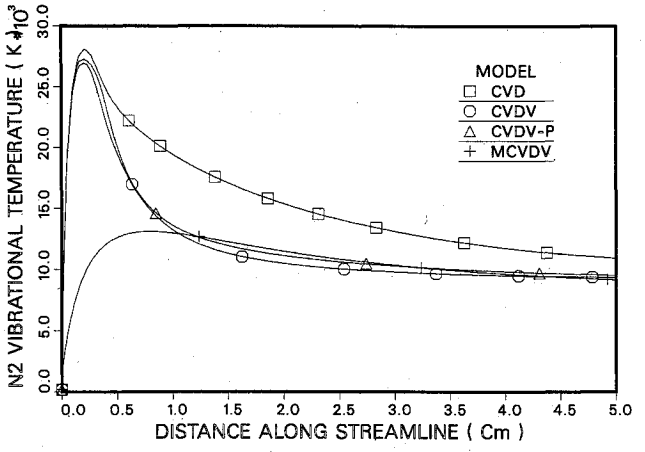

Fig. 10 Effect of vibrational model on T_{vN2} at 10 km/s using RR3 rates.

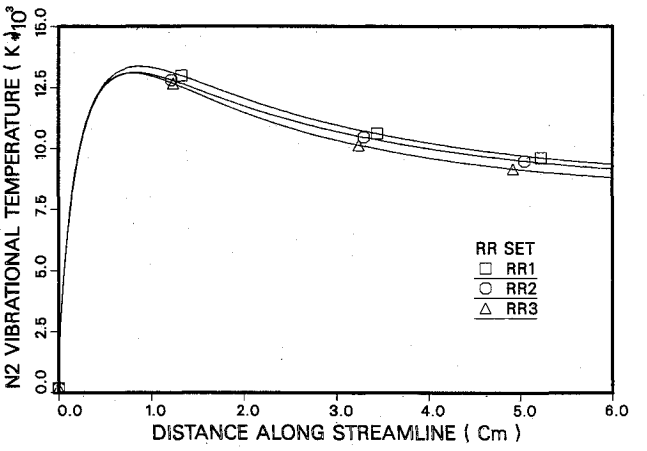

Fig. 11 Effect of reaction rates on T_{vN2} at 10 km/s using MCVDV coupling.

concentrations, however, differ considerably from one reaction set to another; however, the results using MCVDV show smaller differences. Finally, the trends associated with the various vibration-dissociation coupling models are the same as those previously discussed for the 10-km/s case.

Radiative Heat-Transfer Model Studies

In these studies, radiative heat transfer has been computed at 0.25-cm increments out to 10 cm above the axis; for simplicity, details will be discussed only for the body point 9 cm above the axis. Results have been obtained using both the CVDV and MCVDV vibration-dissociation coupling models with the 10-species, 11-reaction chemistry models and three different electron-impact ionization rates. Table 4 presents a partial compilation of some of the numerical results.

Based on the streamline concentration and temperature profiles, most of the flowfield in the stagnation region of the model vehicle will be in chemical nonequilibrium, and the nonequilibrium effects on radiation should be important. The latter are accounted for by correction factors multiplying the equilibrium source functions and absorption coefficients in Eqs. (18), (20), (25), (28), and (29). Figure 14 shows the effect of these correction factors on the radiative heating predictions obtained using CVDV coupling, RR3 rates, and the eight-step absorption coefficients at the entry trajectory point. The prediction without any correction factors is extremely high (2027 W/cm^2), and similar unreasonable results have been observed in all cases. As shown, the imposition of atomic corrections in this case only slightly reduces the prediction, whereas the inclusion of both atomic and molecular corrections significantly

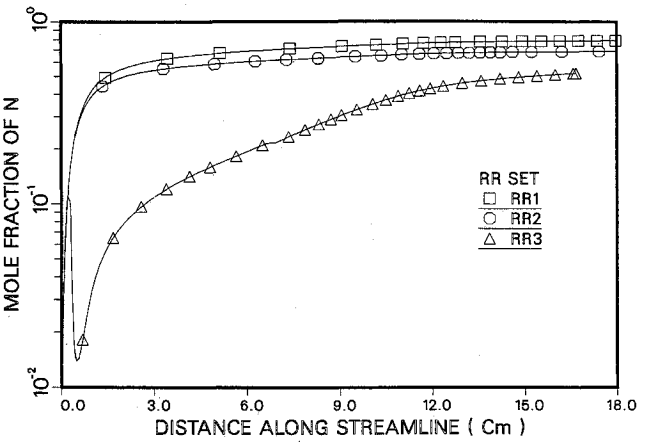

Fig. 12 Effect of reaction rates on N concentration at 10 km/s using CVDV coupling.

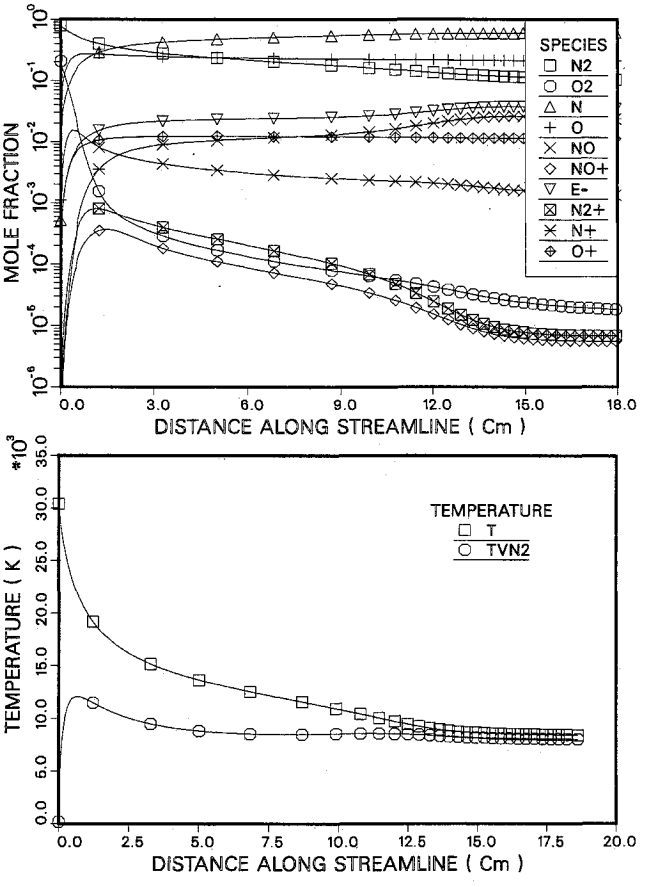

Fig. 13 Species and temperature profiles for MCVDV coupling and RR3 rates at 8.915 km/s.

Table 4 Radiative heat transfer[a]

	CVDV, W/cm^2		MCVDV, W/cm^2	
	Entry	Max-Q	Entry	Max-Q
VUV	11.3	6.38	1.46	0.19
UV and lines	11.2	7.87	2.12	0.35
Vis + IR	6.7	5.20	1.54	0.27
Total	29.2	19.45	5.12	0.81

[a]All at 9 cm above axis for RR3 reaction system with full nonequilibrium radiation corrections.

lowers the predictions. Thus, nonequilibrium radiation effects are very important at this condition, and corrections accounting for the nonexistence of local thermodynamic equilibrium need to be included for both atoms and molecules.

These studies have also shown that the electron-impact ionization rates and the vibration-dissociation coupling models strongly affect the radiation heat transfer. Figure 15 shows radiative heating results obtained using the eight-step model with full radiation correction factors and MCVDV coupling for the three electron-impact ionization rates. The electron-impact rates used in the RR2A (Sandia) and RR2 (Wilson) sets lead to essentially the same prediction, but the Kang-Dunn rate used in the RR3 set gives higher values. The latter occurs because the RR3 electron-impact ionization rate is the fastest and drives the flow toward equilibrium more rapidly, which leads to larger radiation correction factors.

Figure 16 shows the electron temperature distribution between the shock and the wall for the two vibration-dissociation coupling models. As is the case for the streamlines discussed previously, reaction rates have very little effect on the MCVDV T_e profile but strongly affect the CVDV curve. In either case, however, the CVDV electron temperature has a higher peak near the shock wave, which accelerates the ionization rate, drives the flow more rapidly toward equilibrium, and, consequently, as can be seen in Fig. 16, decreases the shock standoff distance. This accelerated rate of ionization, for the case of RR3 rates and CVDV coupling, causes the overshoot shown in Fig. 17 of the N^+ concentration over most of the shock layer. Also shown is the corresponding MCVDV results, which, while having only a small overshoot, is still significantly higher than the values predicted using either the Sandia or Wilson ionization rate.

These enhanced ionization levels in the radiation models, resulting from the RR3 rate set, lead to an increased number of atoms in the excited states, since the latter are in local equilibrium with the ions and electrons. This increase due to nonequilibrium is manifested in the values of the radiation correction factors, which are plotted in Fig. 18 for the RR3 rates and MCVDV coupling. As can be seen, the molecular correction factors are always small, but the atomic corrections are quite large and actually exceed 1 over much of the shock layer. These large values subtly affect the absorption coefficients, optical thicknesses, and the heat transfer via Eq. (6). However, values greater than 1 usually mean that the radiative heating will be greater than that predicted assuming an equilibrium shock layer; thus, for this case, chemical nonequilibrium has led to radiative enhancement.

The choice of vibration-dissociation coupling model also affects the radiative heating in individual wavelength regions. Figure 19 shows by band the radiative heating 9 cm above the axis predicted by the two coupling models. In both cases, the fully corrected eight-step absorption coefficient model and the RR3 reaction set have been used, and, as can be seen, the heating from the MCVDV model is lower in all regions. This lower heating is due to a combination of the lower peak electron temperature and N^+ concentrations predicted by MCVDV. In both cases, the contribution from vacuum ultraviolet (VUV) line centers, band 6, is negligible, indicating that this radiation is intensely absorbed. For both models, about 70% of the total flux to the wall is from the VUV, which is in reasonable agreement with the results of Ref. 4. In addition, an analysis of the spatial origin of the wall flux has been conducted. The analysis shows that, for the CVDV case, most of the wall flux originates in the high electron temperature zone near the shock front, whereas it is from the region next to the body for the MCVDV model.

As stated previously, four absorption coefficient models actually have been used in each case; Fig. 20 compares the fully

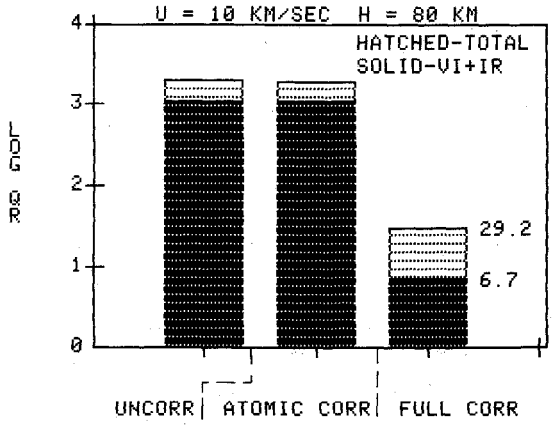

Fig. 14 Effect of radiation correction factors on radiative heating using CVDV coupling and RR3 rates.

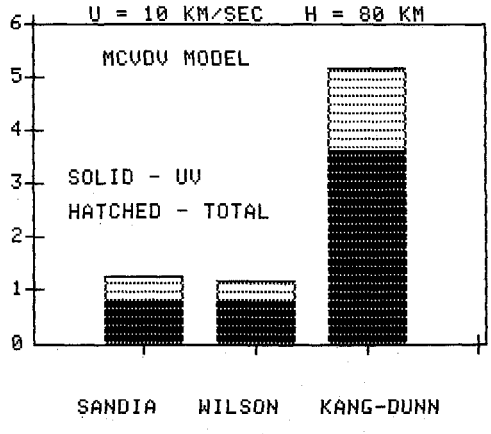

Fig. 15 Effect of electron-impact nitrogen-ionization rate on radiative heating.

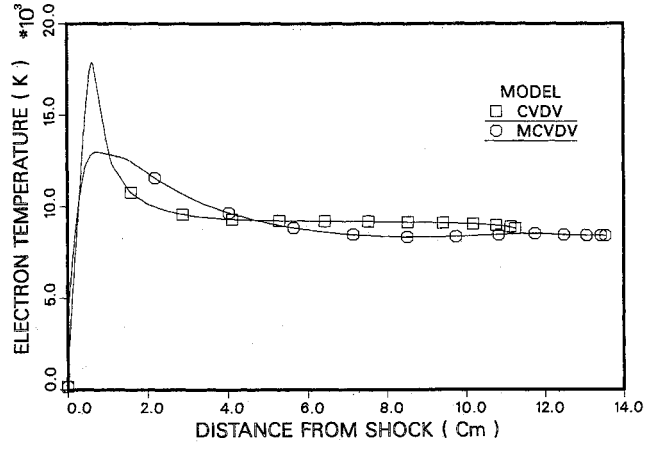

Fig. 16 Effect of vibrational model on T_e between shock and wall at 10 km/s using RR3 rates.

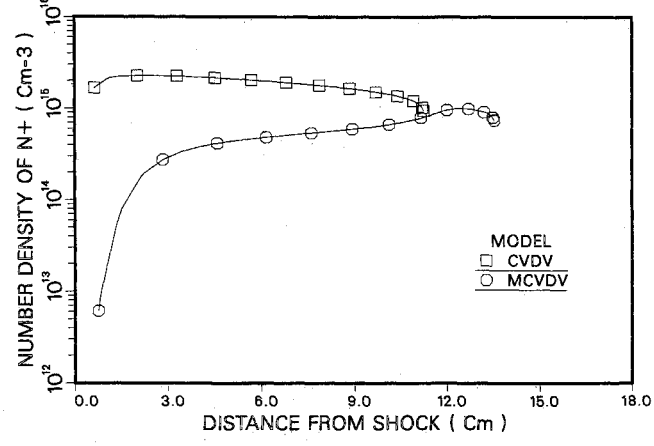

Fig. 17 Effect of vibrational model on N^+ concentration between shock and wall using RR3 rates.

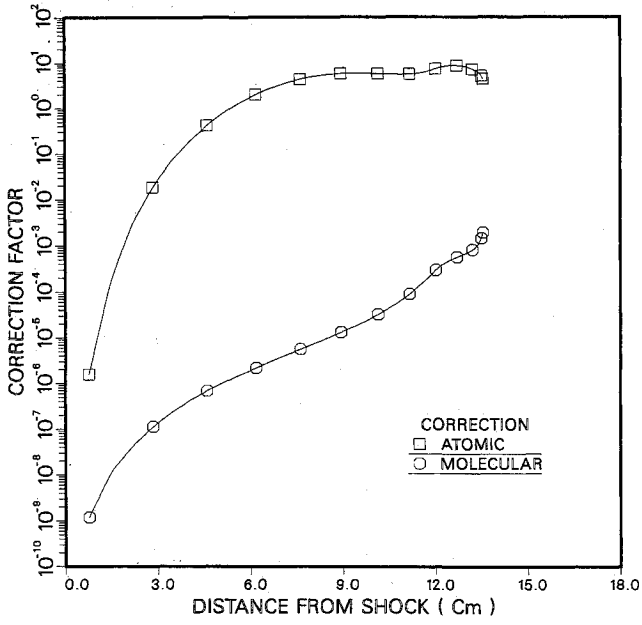

Fig. 18 Nonequilibrium radiation correction factors between shock and wall using RR3 rates and MCVDV coupling.

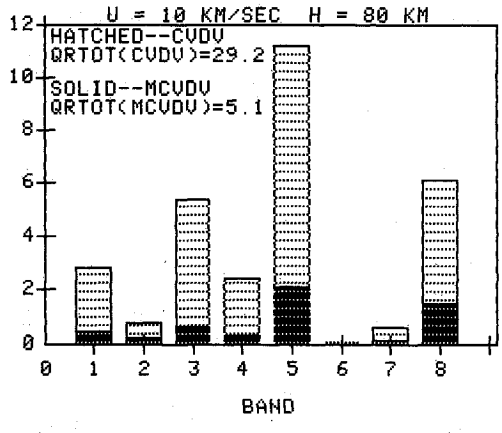

Fig. 19 Effect of vibrational model on radiative heating from individual bands using the eight-step model.

corrected predictions obtained with the RR3 and MCVDV models at the entry point. The ultraviolet prediction from the radiance model, which is transparent, seems excessive, indicating that absorption effects are probably important at these conditions. In addition, although the two-step results in Fig. 20 look reasonable, in general, they have been inconsistent and often unreasonably high. Apparently both the radiance and the two-step models are too simple to adequately represent low-density high-temperature radiating air.

Consequently, Figs. 21 and 22 present comparisons involving the five-and eight-step models. The two models are in good agreement in the visible and IR regions, but differ significantly in the VUV. Examination of the detailed results indicates that these differences result almost entirely from the predictions associated with the VUV lines (band 3 in the five-step model; band 5 and 6 in the eight-step model). As mentioned previously, the five-step model is for atomic nitrogen only; its bandwidths do not correspond physically to the nitrogen spectrum but were selected to yield good agreement with experimental and theoretical data at particular conditions of interest corresponding to lower altitudes.[16] Since the eight-step model has natural bandwidths, is for air, and includes density effects in its line cross sections, it is probably the better of the two models for the present conditions. However, more refined development of VUV line models is definitely needed.

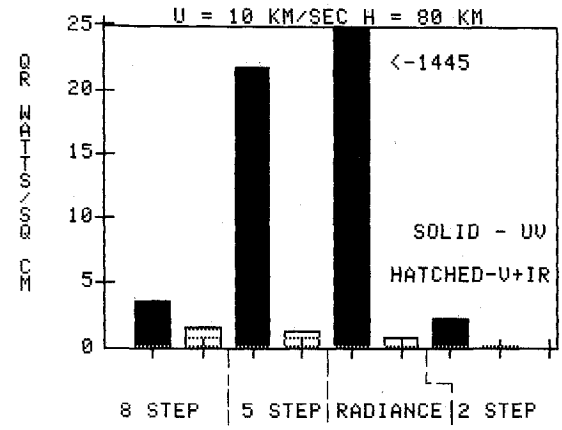

Fig. 20 Comparison of radiative heating predictions by various absorption coefficient models, all with RR3 rates and MCVDV coupling.

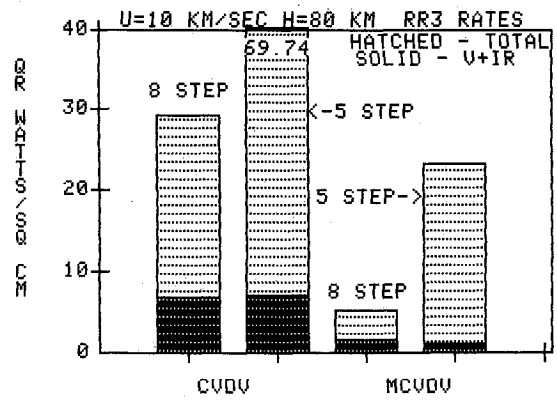

Fig. 21 Comparison of radiative heating by the eight- and five-step models.

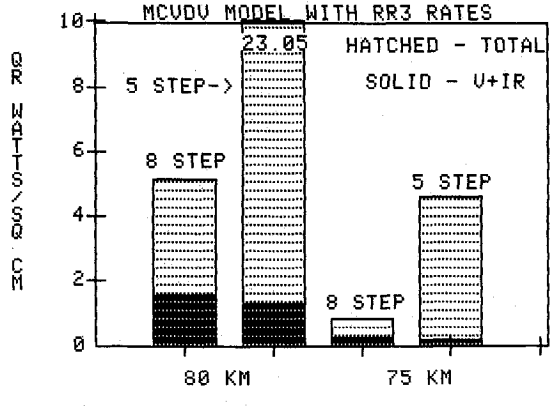

Fig. 22 Comparison of eight- and five-step model radiative heating predictions at entry (80 km) and Max-Q (75 km).

Since these results indicate a significant amount of wall radiative flux in the VUV region, the influence of the vehicle's viscous and thermal boundary layer needs to be considered. Examination of the eight-step model indicates that the cross section for N_2 in the VUV is quite large; thus, significant VUV radiation should be absorbed as molecules appear in the cooler boundary layer. However, if the boundary layer does absorb large amounts of VUV, it will become hotter, optically thinner, and convective heating will increase. Thus, competing effects may result in similar values for total heat transfer. In any event, the effect of the body boundary layer needs further investigation.

Finally, Fig. 22 compares radiative heating predictions at the entry and "max-Q" trajectory points. Although the five-

step VUV results are somewhat suspect, it is interesting to note that both models indicate that peak radiative heating will not occur at the "max-Q" point but will occur at a higher altitude. As shown in Table 4, the CVDV model yields similar results. In addition, an approximate calculation estimates that the equilibrium radiative heating for the 80-km entry point is about 4 W/cm^2; thus, in this case, the present results indicate that nonequilibrium effects lead to an enhancement in radiative heating.

Based on these studies, it is believed that accurate radiative heating results can be obtained by using the eight-step absorption coefficient model, molecular and atomic radiation correction factors, the Kang and Dunn electron-impact nitrogen-ionization rate, and the MCVDV vibration-dissociation coupling model. However, for conservative estimates, the CVDV model could be used in place of the MCVDV coupling scheme to obtain possible "worst-case" estimates.

Conclusions

A series of detailed studies comparing various vibration-dissociation coupling models, reaction systems and rates, and radiative heating models has been conducted for the nonequilibrium stagnation region of an Aeroassisted Flight Experiment/aeroassisted orbital transfer vehicle. Based on these studies, the following conclusions can be made:

1) At the exit trajectory point, simplified reaction schemes yield useful results at significant computational savings, providing that ionized species are not of interest.

2) A modified coupled vibration-dissociation-vibration (MCVDV) scheme has been shown to yield reasonable vibrational and electron temperature profiles as well as species concentration variations.

3) At entry and max-Q trajectory points, detailed reaction systems are required to predict properly the charged species affecting the radiative heat transfer. In addition, the results are sensitive to the nitrogen-ionization electron-impact rate. Further study is needed to properly model ionization chemistry.

4) Nonequilibrium effects significantly affect the radiative heat transfer, and both molecular and atomic nonequilibrium radiation correction factors are essential for proper predictions. However, radiative cross sections and absorption coefficient step models based on equilibrium results can be used provided nonequilibrium corrections are included.

5) The treatment of line radiation at the low-density Aeroassisted Flight Experiment conditions needs further study and refined radiation step models need to be developed.

6) Accurate radiative heating predictions can probably be obtained by combining an eight-step absorption coefficient model, radiation correction factors, the Kang and Dunn electron-impact nitrogen-ionization rate, and the MCVDV coupling model. However, conservative results can be obtained by using the CVDV model instead of MCVDV.

Acknowledgment

This effort was primarily supported under a subportion of NASA Grant NAG 9-192 from the NASA Johnson Space Center, with Dr. Carl Scott, Aerosciences Branch, as the technical monitor.

References

[1]Gnoffo, P. and Greene, F. A., "A Computational Study of the Flowfield Surrounding the Aeroassist Flight Experiment Vehicle," AIAA Paper 87-1575, June 1987.

[2]Park, C., "Assessment of Two-Temperature Kinetic Model for Ionizing Air," AIAA Paper 87-1574, June 1987.

[3]Grosse, W. L., "A Thin Shock Layer Solution for Nonequilibrium, Inviscid Flows in Earth, Martian, and Venusian Atmospheres," NASA TN D-6529, Dec. 1971.

[4]Moss, J. N., Bird, G. A., and Dogra, V. K., "Nonequilibrium Thermal Radiation for an Aeroassist Flight Experiment Vehicle," AIAA Paper 88-0081, Jan. 1988.

[5]Wilson, J., "Ionization Rate of Air Behind High Speed Shock Waves," *Physics of Fluids,* Vol. 9, Oct. 1966, pp. 1913–1921.

[6]Carlson, L. A., "Radiative Gasdynamic Coupling and Nonequilibrium Effects behind Reflected Shock Waves," *AIAA Journal,* Vol. 9, May 1971, pp. 858–865.

[7]Marrone, P. V., "Inviscid, Nonequilibrium Flow Behind Bow and Normal Shock Waves, Part I. General Analysis and Numerical Examples," Cornell, Buffalo, NY, Cornell Aeronautical Rept. QM-1626-A-12(I), May 1963.

[8]Carlson, L. A. and Rieper, R. G., "Electron Temperature and Relaxation Phenomena Behind Shock Waves," *Journal of Chemical Physics,* Vol. 57, No. 2, July 1972, pp. 760–766.

[9]Kang, S. W. and Dunn, M. G., "Theoretical and Measured Electron-Density Distributions for the Ram Vehicle at High Altitudes," AIAA Paper 72-689, June 1972.

[10]Carnicom, M. L., "Reaction Rates for High Temperature Air," Sandia Rept. SC-R-66-885, May 1966.

[11]Treanor, C. E. and Marrone, P. V., "Effect of Dissociation on the Rate of Vibrational Relaxation," *Physics of Fluids,* Vol. 5, Sept. 1962, pp. 1022–1026.

[12]Hammerling, P., Teare, J. D., and Kivel, B., "Theory of Radiation from Luminous Shock Waves in Nitrogen," *Physics of Fluids,* Vol. 2, No. 4, July-Aug. 1959, pp. 422–426.

[13]Park, C., "Assessment of a Two Temperature Kinetic Model for Dissociating and Weakly Ionizing Nitrogen," *Journal of Thermophysics and Heat Transfer,* Vol. 2, Jan. 1988, pp. 8–16.

[14]Lee, J. H., "Electron Impact Vibrational Excitation Rates in Flowfield of Aeroassisted Orbital Transfer Vehicles," *Progress in Astronautics and Aeronautics: Thermophysical Aspects of Re-Entry Flows,* Vol. 103, edited by J. N. Moss and C. D. Scott, AIAA, New York, 1986, pp. 197–224.

[15]Millikan, R. C. and White, D. R., "Systematics of Vibrational Relaxation," *Journal of Chemical Physics,* Vol. 39, Dec. 1963, pp. 3209–3213.

[16]Knott, P. R., Carlson, L. A., and Nerem, R. M., "A Further Note on Shock Tube Measurements of End Wall Radiative Heat Transfer in Air," *AIAA Journal,* Vol. 7, Nov. 1969, pp. 2170–2172.

[17]Olstad, W. B., "Nongray Radiating Flow about Smooth Symmetric Bodies," *AIAA Journal,* Vol. 9, Jan. 1971, pp. 122–130.

[18]Nicolet, W. E., "Advanced Methods for Calculating Radiation Transport in Ablation Product Contaminated Boundary Layers," NASA CR-1656, Sept. 1970.

[19]Park, C., "Calculation of Nonequilibrium Radiation in AOTV Flight Regimes," AIAA Paper 84-0306, Jan. 1984.

[20]Chapin, C. E., "Nonequilibrium Radiation and Ionization in Shock Waves," AA&ES 67-9, Purdue Univ., Lafayette, IN, June 1967.

[21]Clarke, J. H. and Ferrari, C., "Gas Dynamics with Nonequilibrium Radiative and Collisional Ionization," *Physics of Fluids,* Vol. 8, Dec. 1965, pp. 2121–2139.

[22]Park, C., "Radiation Enhancement by Nonequilibrium in Earth's Atmosphere," AIAA Paper 83-0410, Jan. 1983.

[23]Cauchon, D. L., McKee, C. W., and Cornette, E. S., "Spectral Measurements of Gas Cap Radiation During Project Fire Flight Experiments at Reentry Velocities near 11.4 Km/Sec," NASA TM X-1380, Oct. 1967.

[24]Curtiss, J. T. and Strom, C. R., "Computations of the Nonequilibrium Flow of a Viscous, Radiating Fluid About a Blunt Axisymmetric Body," Air Force Flight Dynamics Lab., Wright-Patterson AFB, OH, AFFDL-TR-67-40, Vol. 1, June 1967.

[25]Anderson, J. D., Jr., "Heat Transfer from a Viscous Nongray Radiating Shock Layer," *AIAA Journal,* Vol. 6, Aug. 1968, pp. 1570–1573.

[26]Allen, R. A., "Nonequilibrium Shock Front Rotational, Vibrational and Electronic Temperature Measurements," NASA CR-205, April 1965.